Functionalized Vertically Aligned Carbon Nanofibers as Scaffolds for Immobilization and Electrochemical Detection of Redox-Active Proteins

Sarah E. Baker, Paula E. Colavita, Kiu-Yuen Tse, and Robert J. Hamers*

Department of Chemistry, University of Wisconsin—Madison, 1101 University Avenue, Madison, Wisconsin 53706

Received April 18, 2006. Revised Manuscript Received June 28, 2006

We have investigated the functionalization of vertically aligned carbon nanofibers with the redox-active protein cytochrome *c* and have characterized the resulting chemical and electrochemical activity. A comparison of monolayers with different terminal groups shows that those exposing carboxylic acid groups are most effective at binding active cytochrome *c* to carbon nanofibers. Cyclic voltammetry (CV) measurements reveal redox peaks due to electrochemical activity of the nanofiber-bound protein. CV and chemical measurements of enzymatic activity both show that nanofibers modified with cytochrome *c* yield approximately 10 times more activity than similarly modified surfaces of glassy carbon and gold. However, cytochrome *c*-modified nanofibers yield a high capacitive background, reducing the signal-to-noise ratio of the electrical measurements. We attribute this in part to inhomogeneous functionalization of the nanofibers at edge-plane versus basal-plane sites on the nanofiber surface, leading to leaky monolayers that yield increased capacitance. Our results demonstrate the ability to link chemically and electrochemically active proteins to nanofibers in a manner that preserves their activity and provide insight into the nanometer-scale factors that control the resulting chemical and electrochemical properties of biologically modified nanostructured electrodes.

Introduction

Vertically aligned carbon nanofiber (VACNF) electrodes are a relatively new class of carbon-based materials.[1−4] Their high chemical stability, high degree of biologically accessible surface area,[5] vertical orientation, nanoscale dimension, and ease of patterning them[6,7] make VACNFs interesting substrates for development as scaffolds for biological detection. Additionally, they have been shown to have the mechanical strength and sufficiently narrow diameter to penetrate cells, making them suitable for intracellular electrochemical detection.[8]

Cytochrome *c* (cyt *c*) is a small electron-transfer metalloprotein whose electrochemistry has been widely studied in part because of its stability and capacity for direct charge transfer with promoter-modified electrodes. In fact, cyt *c* has become a model system for adapting electrode surfaces for globular proteins.[9−12] The optimization of charge transfer between protein and electrode through immobilization removes the rate-limiting step of diffusion and can aide in the understanding of the mechanism, protein orientation, and charge-transfer kinetics as well as in the design and development of biosensors and biomaterials.[13,14]

Cyt *c*-modified electrodes have been used successfully for the detection of superoxides, which are implicated in several medical conditions including cardiovascular disease and arthritis.[13,15,16] Additionally, surface-immobilized cyt *c* has been used for energy conversion in biofuel and photoelectrochemical cells.[13,17] Finally, there is increasing interest in immobilization of proteins and enzymes onto mesoporous and/or high surface area supports for industrial applications, due to the increased stability and activity upon immobilization as well as the high loading afforded by high surface area materials.[18−20]

We have chemically modified VACNF forests for direct charge transfer with cyt *c*. The loading and electrochemical

* Corresponding author. E-mail: rjhamers@wisc.edu.

(1) Chen, Y.; Wang, Z. L.; Yin, J. S.; Johnson, D. J.; Prince, R. H. *Chem. Phys. Lett.* **1997**, *272*, 178.
(2) Ren, Z. F.; Huang, Z. P.; Xu, J. W.; Wang, J. H.; Bush, P.; Siegal, M. P.; Provencio, P. N. *Science* **1998**, *282*, 1105.
(3) Meyyappan, M.; Delzeit, L.; Cassell, A.; Hash, D. *Plasma Sources Sci. Technol.* **2003**, *12*, 205.
(4) Melechko, A. V.; Merkulov, V. I.; McKnight, T. E.; Guillorn, M. A.; Klein, K. L.; Lowndes, D. H.; Simpson, M. L. *J. Appl. Phys.* **2005**, *97*, 041301.
(5) Baker, S.; Tse, K.-Y.; Hindin, E.; Nichols, B. M.; Clare, T. L.; Hamers, R. J. *Chem. Mater.* **2005**, *17*, 4971.
(6) Lee, C.-S.; Baker, S. E.; Marcus, M. S.; Yang, W.; Eriksson, M. A.; Hamers, R. J. *Nano Lett.* **2004**, *4*, 1713.
(7) Guillorn, M. A.; McKnight, T. E.; Melechko, A.; Merkulov, V. I.; Britt, P. F.; Austin, D. W.; Lowndes, D. H.; Simpson, M. L. *J. Appl. Phys.* **2002**, *91*, 3824.
(8) McKnight, T. E.; Melechko, A. V.; Hensley, D. K.; Mann, D. G. J.; Griffin, G. D.; Simpson, M. L. *Nano Lett.* **2004**, *4*, 1213.
(9) Leopold, M. C.; Bowden, E. F. *Langmuir* **2002**, *18*, 2239.
(10) Strauss, E.; Thomas, B.; Yau, S.-T. *Langmuir* **2004**, *20*, 8768.
(11) Chen, X.; Ferrigno, R.; Yang, J.; Whitesides, G. M. *Langmuir* **2002**, *18*, 7009.
(12) Song, S.; Clark, R. A.; Bowden, E. F.; Tarlov, M. J. *J. Phys. Chem.* **1993**, *97*, 6564.
(13) Willner, I.; Katz, E. *Bioelectronics: from theory to applications*; Wiley-VCH: Weinheim, 2005.
(14) Holt, K. B. *Langmuir* **2006**, *22*, 4298.
(15) Krylov, A. V.; Beissenhirtz, M.; Adamzig, H.; Scheller, F. W.; Lisdat, F. *Anal. Bioanal. Chem.* **2004**, *378*, 1327.
(16) Beissenhirtz, M. K.; Scheller, F. W.; Lisdat, F. *Anal. Chem.* **2004**, *76*, 4665.
(17) Astuti, Y.; Palomares, E.; Haque, S. A.; Durrant, J. R. *J. Am. Chem. Soc.* **2005**, *127*, 15120.
(18) Hartmann, M. *Chem. Mater.* **2005**, *17*, 4577.
(19) Hudson, S.; Magner, E.; Cooney, J.; Hodnett, B. K. *J. Phys. Chem. B* **2005**, *109*, 19496.
(20) El Kasmi, A.; Wallace, J. M.; Bowden, E. F.; Binet, S. M.; Linderman, R. J. *J. Am. Chem. Soc.* **1998**, *120*, 225.

10.1021/cm0609000 CCC: $33.50
Published on Web 08/04/2006

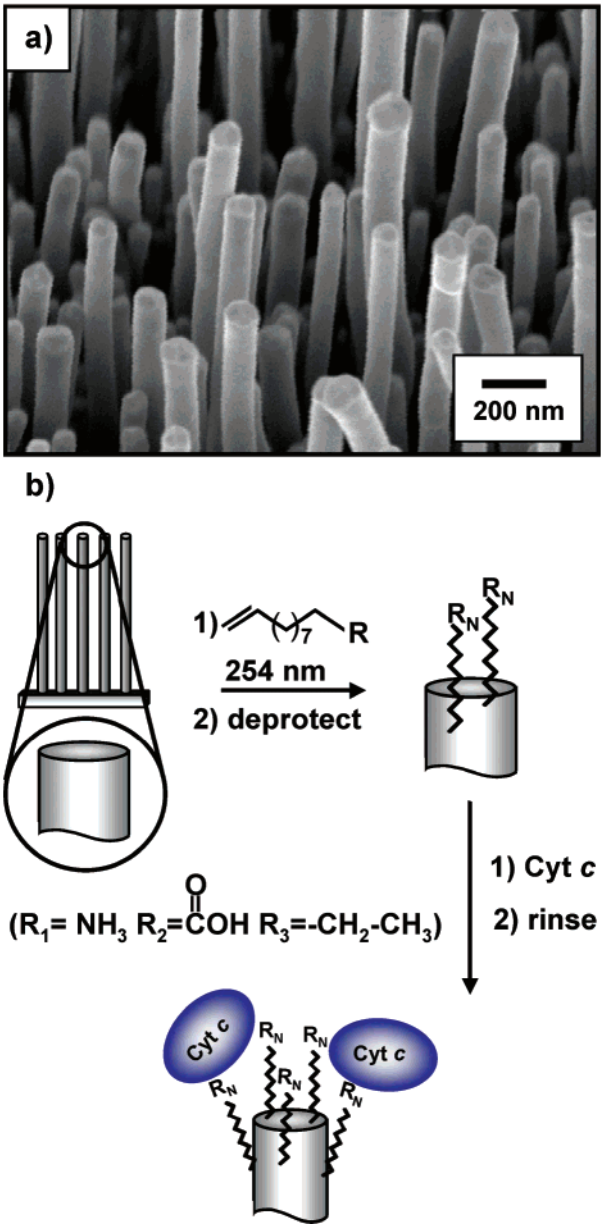

Figure 1. (a) SEM image (taken at a 25° tilt) of a VACNF substrate. (b) Schematic of VACNF functionalization.

characteristics of the immobilized cyt *c* on VACNFs are compared to chemically modified glassy carbon and gold to understand and optimize the properties of VACNF electrodes as a platform for biological detection.

Experimental Section

Substrate Preparation. The VACNF, glassy carbon, and gold substrates were prepared prior to functionalization as follows: VACNFs were grown on highly doped n-type silicon substrates covered with evaporated layers of 50 nm molybdenum, 20 nm titanium as a wetting layer, and 20 nm nickel as a top catalyst layer. These substrates were then placed in a custom-built direct current plasma-enhanced chemical vapor deposition chamber similar to one described previously,[21] and nanofibers were grown for 15 min at 4 Torr and 360 W under a flow of 100 sccm ammonia and 35 sccm acetylene gases. Figure 1a shows a scanning electron microscopy (SEM) image of the resulting VACNF substrates; this image was obtained with the sample tilted by 25°. Under the growth conditions used here the nanofibers are 2−3 μm in length, with diameters of 80 ± 20 nm measured by SEM. Transmission electron microscopy (TEM) images (not shown) reveal that the nanofibers show crystalline graphite planes tilted at a small angle of ∼10° with respect to the fiber axis; this tilt angle provides for significant amounts of the graphite edge plane to be exposed along the side walls. The glassy carbon substrates were first cleaned in a piranha bath[22] rinsed with water and placed in a home-built RF hydrogen plasma chamber for hydrogen termination before functionalization. Evaporated gold-on-glass substrates were cleaned by placement under a UV lamp (254 nm) for 30 min and by rinsing with 200 mL of water followed by 200 mL of ethanol.

Substrate Functionalization. In previous studies we have shown that carbon-based materials such as diamond,[23,24] glassy carbon,[25] and carbon nanofibers[5] can be functionalized by reacting them with liquid-phase molecules containing an alkene (C═C) group and inducing the reaction with ultraviolet light. Figure 1b depicts this functionalization method. A drop of the an alkene (terminated at the opposite end with one of several different groups R_1, R_2, or R_3, as depicted in Figure 1b) was applied to the surfaces, followed by placing a quartz window over each substrate to prevent drying during the reaction. These substrates were placed in a nitrogen-purged chamber with a quartz lid and illuminated with a low-pressure mercury lamp emitting 254 nm light for ∼16 h. In additional experiments not described here, we used X-ray photoelectron spectroscopy to characterize the rate of functionalization and found that the 16 h exposure time used here is sufficient for the reactions to reach completion. After functionalization was complete, the substrates were rinsed with chloroform and methanol. The amine and carboxylic acid terminations were achieved by using the protected form of the molecules [*tert*-butyloxy-carbamate (tBOC) and methyl ester, respectively] during the UV step to inhibit possible side reactions and were deprotected after rinsing.

To produce surfaces terminated with carboxylic acid groups, the methyl ester-protected undecylenic acid was used during the UV reaction and then deprotected by placing the methyl ester-terminated chip into a slurry of 250 mM potassium *t*-butoxide (Aldrich) in dimethyl sulfoxide for 6 min, followed by rinsing with 0.1 M HCl and then deionized water.[26,27]

To produce surfaces terminated with primary amines, tBOC-protected 10-amino-dec-1-ene was linked to the surface during the UV step. After the UV reaction, the amine was deprotected by immersing the substrate in 1:1 trifluoroacetic acid/methylene chloride for 1 h, followed by immersion in 10% ammonium hydroxide and rinsing with deionized water.[5] The alkane termination was achieved using dodecene as the neat alkene and did not require a deprotection step.

The clean gold surfaces were functionalized with carboxylic acid groups by immersing them in a 4 mM solution of 11-mercaptoundecanoic acid (MUA) in nitrogen purged ethanol in the dark for 24−48 h, followed by rinsing with ethanol and drying under a stream of nitrogen.

(21) Cassell, A. M.; Ye, Q.; Cruden, B. A.; Li, J.; Sarrazin, P. C.; Ng, H. T.; Han, J.; Meyyappan, M. *Nanotechnology* **2004**, *15*, 9.
(22) Twenty minutes at room temperature in 3:1 H_2SO_4 (concd)/H_2O_2 (30%).
(23) Yang, W. S.; Auciello, O.; Butler, J. E.; Cai, W.; Carlisle, J. A.; Gerbi, J. E.; Gruen, D. M.; Knickerbocker, T.; Lasseter, T. L.; Russell, J. N., Jr.; Smith, L. M.; Hamers, R. J. *Nat. Mater.* **200**2, *1*, 253.
(24) Nichols, B. M.; Butler, J. E.; Russell, J. N., Jr.; Hamers, R. J. *J. Phys. Chem. B* **2005**, *109*, 20938.
(25) Lasseter, T. L.; Cai, W.; Hamers, R. J. *Analyst* **2004**, *129*, 3.
(26) Chang, F. C.; Wood, N. F. *Tetrahedron Lett.* **1964**, *40*, 2969.
(27) Strother, T.; Cai, W.; Zhao, X.; Hamers, R. J.; Smith, L. M. *J. Am. Chem. Soc.* **2000**, *122*, 1205.

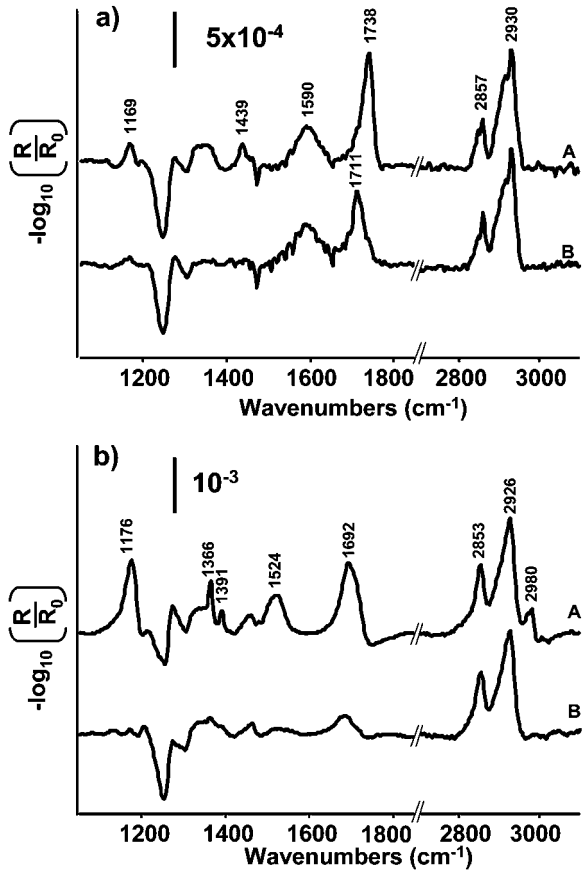

Figure 2. (a) IRRAS spectra of undecylenic acid−methyl ester functionalized VACNFs (top) and the same sample after deprotection (bottom). (b) tBOC-protected 10-amino-dec-1-ene functionalized VACNFs (top) and the same sample after deprotection (bottom).

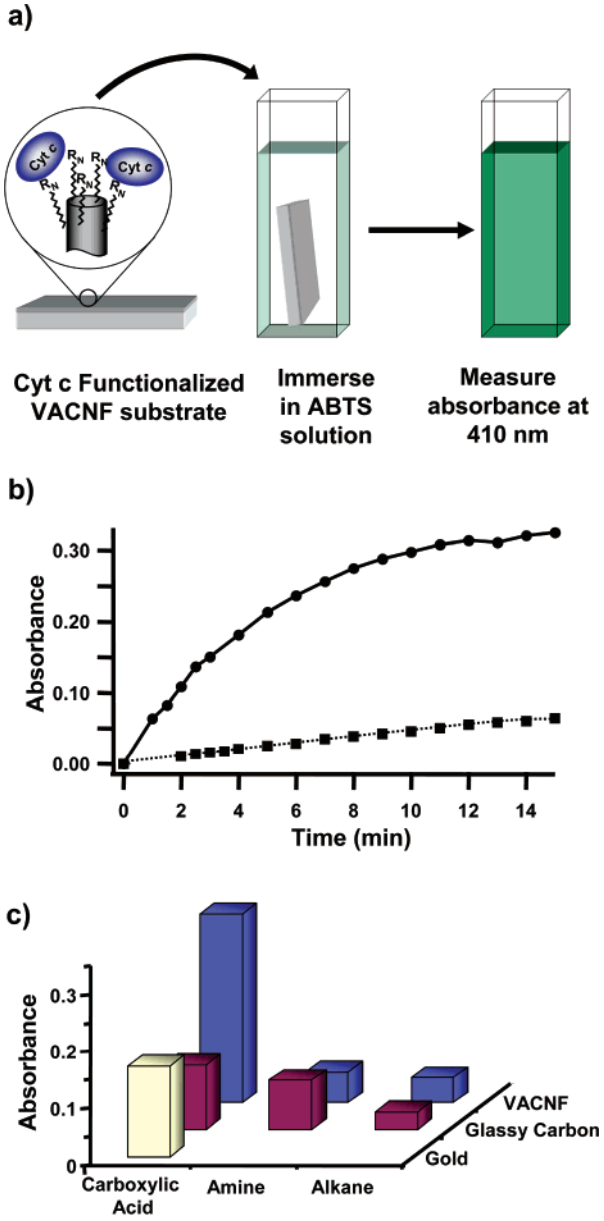

Figure 3. (a) Sequence of steps used in ABTS assay for determining relative cyt *c* loading on surfaces. (b) Absorbance at 410 nm as a function of time due to ABTS oxidation on cyt *c* functionalized VACNFs (solid line) and glassy carbon (dotted line). (c) Absorbance values at 410 nm for VACNF, glassy carbon, and gold surfaces with carboxylic acid, alkane, and amine terminations after ABTS assay.

Colorimetric Protein Loading Assay. To monitor the relative amounts of active cyt *c* on each of the different surfaces, we immobilized cyt *c* on the surfaces by applying a 20 μL droplet of a 0.8 mg/mL solution of horse heart cyt *c* (Sigma) in 0.44 mM argon-purged potassium phosphate buffer (PB, pH 7.4) to each 40 mm^2 chip in a humid chamber in the dark for 45 min. The chips were then each rinsed for 30 s with 0.44 mM PB from a wash bottle and placed wet into 500 μL of an 2,2′-Azinobis[3-ethylbenzothiazoline-6-sulfonic acid]-diammonium salt solution (one-step ABTS, pierce). After 40 min, 400 μL of each of the ABTS solutions was removed and placed in a cuvette containing 400 μL of 1% sodium dodecyl sulfate. The absorbance of each solution was then measured at 410 nm, using a path length of 0.5 cm. This sequence of steps is illustrated in Figure 3A.

Control experiments demonstrated that the color change that was measured in the solution was due to the surface-immobilized protein oxidizing the ABTS molecules, rather than to the protein first leaching off of the electrode surfaces and into solution before oxidizing the ABTS. Two VACNF chips, A and B, were modified with undecylenic acid, immobilized with cyt *c*, and rinsed as described in the text. Chip A was placed directly in 400 μL of ABTS solution (ionic strength 0.1 M, pH ∼5.3), and after 45 min the ABTS solution was removed and added to 400 μL of 0.44 mM PB (0.1 M, pH 5.3) in a cuvette. The UV/vis absorbance of this solution at 410 nm was 0.318. Chip B was placed directly into 400 μL of PB (0.1 M, pH 5.3) instead of ABTS for 45 min to measure the amount of cyt *c* that leaches from the surface into solution over a 45-min period. This PB was then removed and added to 400 μL of ABTS for another 45 min. The absorbance of this solution at 410 nm was only 0.056. Thus, we conclude that the vast majority of the absorbance measured in the solution phase on carboxylic acid-terminated VACNFs (0.318) was due to surface-immobilized cyt *c*.

Electrochemical Measurements. The electrochemical measurements were conducted using a Solartron 1287 electrochemical interface in a three electrode cell with the working and counter electrode areas defined by a poly(dimethyl siloxane) gasket (∼2 mm diameter circle) equipped with Teflon tubing for the flow of electrolyte. Functionalized gold, glassy carbon, or VACNFs served as the working electrodes, Pt foil served as the counter electrodes, and Ag/AgCl wire served as the reference electrode. All electrochemical measurements were performed in a PB solution consisting of a 4.4 mM total phosphate concentration, adjusted to pH 7.0 with HCl; this yields a [Cl$^-$] of approximately 2 mM. Background cyclic voltammetry scans were measured on the functionalized surfaces before cyt *c* adsorption. After acquiring stable background spectra, a solution of 0.8 mg/mL cyt *c* in 0.44 mM PB was introduced to

the electrochemical cell using a syringe pump and was allowed to bind to the working electrode for ~30 min. The electrodes were then rinsed with 4.4 mM PB flowing at 0.1 mL/min for 5−10 min. Cyclic voltammograms were recorded again, this time reflecting the electrochemistry of adsorbed cyt *c*. All potentials are referenced to the embedded Ag/AgCl electrode. Because in the microfluidic cell the concentration of Cl^- is ~2 mM, however, the reference electrode has a potential that is approximately 150 mV more positive than a conventional Ag/AgCl reference electrode.

Fourier Transform Infrared (FTIR) Measurements. The UV attachment of the alkenes to VACNFs and subsequent chemical modifications were verified by infrared reflection−absorption spectroscopy (IRRAS). Relatively "short" fibers 500 nm long were used for the IRRAS characterization. Spectra were collected on a Bruker Vector 33 FTIR spectrometer using a variable angle reflectance accessory (VeeMaxII, Pike) equipped with a wire grid polarizer. Spectra shown here were obtained at 60 and 30° incidence angles, using p-polarized light; 500 scans at 4 cm^{-1} resolution were collected for both the background and the sample. Spectra were baseline-corrected using a commercial software program (WinFirst) and offset for clarity.

Results

IRRAS Characterization of VACNFs. Figure 2 shows the IRRAS spectra of the VACNFs, after grafting of the alkene and following their deprotection, for the undecylenic acid methyl ester (a) and the tBOC-protected 10-amino-dec-1-ene (b). All spectra shown were measured using a 60° incidence angle (with respect to the substrate normal) and p-polarized light.

The IRRAS spectrum of nanofibers functionalized with the methyl ester (Figure 2a, trace A) contains several peaks. The most significant of these are the prominent peaks at 2857 and 2930 cm^{-1}, a large peak at 1738 cm^{-1}, and small sharp peaks at 1439 and 1169 cm^{-1}. While a detailed assignment has not been performed, on the basis of previous measurements of gold surfaces modified with a similar ester it is possible to assign the most prominent peaks.[28,29] The peaks at 2857 and 2930 cm^{-1} arise from the symmetric and asymmetric modes of CH_2 groups. The ester methyl group contribution is not resolved and appears as a small shoulder of the methylene asymmetric stretch. The large peak at 1738 cm^{-1} arises from the C═O stretch of the carbonyl group of the ester, and the peak at 1439 cm^{-1} is attributed to the symmetric bending mode of CH_3. The peak at 1169 cm^{-1} corresponds to the C—O stretch of the ester group.[28,29]

The IRRAS spectra of functionalized fibers also show peaks that can be attributed to the VACNF substrate. Peaks that are associated with the fibers in Figure 2a are a negative peak present at 1246 cm^{-1} and a positive broad peak at 1590 cm^{-1}. The peak at 1246 cm^{-1} likely arises from metal oxides (specifically molybdenum and/or titanium) present under the VACNF layer. The broad feature at 1590 cm^{-1} is not present on freshly grown bare fibers, but it increases as the fibers are exposed to the laboratory atmosphere for several days or when fibers are immersed in organic solvents such as methanol. We ascribe this feature to the oxidation of surface sites, possibly to primary amines on the surface, or to the infrared active vibrational mode E_{1u} of the graphene sheets within the fibers.

After deprotection (Figure 2a, trace B), the C═O stretching peak at 1738 cm^{-1} shifts downward in frequency to 1711 cm^{-1}, the peak at 1439 cm^{-1} disappears, and the peak at 1169 cm^{-1} is greatly reduced, while the features in the C—H stretching region are not significantly altered. The 27 cm^{-1} downward shift in frequency of the C═O stretch is similar to that observed in other systems, with the acids typically showing C═O vibrational frequencies lower than the corresponding esters.[28,29] The decrease in intensity of the peaks at 1439 cm^{-1} (CH_3 symmetric bending) and 1169 cm^{-1} (C—O stretch) also correspond to the deprotection of a carboxylic acid group.

In the case of the tBOC-protected 10-amino-dec-1-ene (Figure 2b) the IRRAS spectrum displays the characteristic absorbances of a carbamate group (trace A): a carbonyl stretch at 1692 cm^{-1}, a CHN group vibration at 1520 cm^{-1}, and a C—O stretching vibration at 1176 cm^{-1}.[29] Also, vibrations associated to *tert*-butyl CH_3 stretching (2980 cm^{-1}) and bending (1391 cm^{-1}, 1366 cm^{-1}) are clearly visible.[29] All of these modes are either greatly reduced or disappear altogether upon deprotection of the amine terminal group (trace B).

The FTIR measurements demonstrate that the photochemical functionalization is an effective way to modify nanofibers with functional groups of interest.

Loading of Cyt *c* on VACNF, Glassy Carbon, and Gold Surfaces. To identify how the functionalization of nanofibers with different molecular species affected the loading of active cyt *c* onto the fibers, we used a colorimetric assay based on the oxidation of ABTS[19] by cyt *c* in the presence of hydrogen peroxide.[30] Experiments were performed on carbon nanofibers and glassy carbon surfaces that were modified to expose different functional groups; these groups included primary amines ($-NH_2$), carboxylic acid (−COOH), and saturated alkyl groups. The loading of cyt *c* on carboxylic acid (MUA)-terminated gold was used as a point of comparison, because the interaction of gold surfaces with cyt *c* has been extensively studied and its electrochemistry is well-understood.[9,11,12,14,20,31]

Figure 3b shows the absorbance values from the interaction of ABTS with the surfaces of carbon nanofibers (solid line) and glassy carbon (dotted line) as a function of time, both of which were covalently modified with carboxylic acid groups and then cyt *c*. It is clear that the nanofiber surface yields a much higher initial rate of reaction. During the first 3 min, the rate of reaction (obtained by taking the slope of the data in Figure 3b) on nanofibers is 10 times that observed for the glassy carbon surface. At longer times, the absorbance versus time plot for the nanofibers levels out, which may be due to diffusion limitations to the electrode surface or due to inhibition of the redox activity by the buildup of oxidized ABTS in the solution. In practical applications, either the

(28) Nuzzo, R. G.; Dubois, L. H.; Allara, D. L. *J. Am. Chem. Soc.* **1990**, *112*, 558.
(29) Socrates, G. *Infrared and Raman Characteristic Group Frequencies*, 3rd ed.; Wiley: Chichester, 2001.
(30) Deere, J.; Magner, E.; Wall, J. G.; Hodnett, B. K. *Biotechnol. Prog.* **2003**, *19*, 1238.
(31) Collinson, M.; Bowden, E. F.; Tarlov, M. J. *Langmuir* **1992**, *8*, 1247.

Table 1. Absorbance Values Measured at 410 nm Due to Oxidized ABTS, Indicating Relative Active Cyt *c* Loading after 40 min on VACNF, Glassy Carbon, and Gold with Different Surface Terminations

functionalization	VACNF (3 trials)	glassy carbon	gold
amine	0.054 ± 0.002	0.088	
alkane	0.044 ± 0.010	0.032	
carboxylic acid	0.327 ± 0.018	0.115	0.161

short-time or the long-time behavior could be of interest. The short-time behavior shows that the cyt *c*-modified nanofibers have very high enzymatic activity. The longer-time behavior shows that the very high surface area that nanofiber electrodes present may not necessarily be realized if other processes, such as diffusion, become important.

To compare the enzymatic activity of cyt *c* on various surfaces terminated with different functional groups, we measured the long-time behavior after 40 min of activity. These absorbance values are tabulated in Table 1 and are shown graphically in Figure 3c. In the figure, the *x* axis of the plot indicates the surface termination, the *y* axis represents the different materials that were modified, and the *z* axis represents the raw absorbance values due to ABTS which has been oxidized by surface-bound cyt *c*. The carboxylic acid-modified surfaces of all three materials (and especially of VACNFs) show the highest levels of ABTS absorption and, therefore, reflect the highest levels of enzymatic activity. The amine- and alkane-modified surfaces both show comparatively low activity. While the detailed origin of these differences has not been investigated, previous studies have shown that proteins are often denatured at hydrophobic surfaces;[11] thus, we expect that the low activity of the alkane-modified surfaces is likely associated with their hydrophobicity. We attribute the high activity on acid-terminated surfaces and low activity on amine-terminated surfaces to electrostatic interactions of cyt *c* with these surfaces. Because the isoelectric point (pI) of cyt *c* is near pH 10,[32] it is positively charged at pH 7.4; therefore, electrostatic interactions lead to favorable binding to the (negatively charged) acid-terminated surfaces and disfavor binding to the (positively charged) amine-terminated surfaces.

The data in Figure 3c show that functionalization with carboxylic acid groups leads to the highest overall enzymatic activity, while surfaces terminated with neutral (alkane) or positively charged (amine) groups show much less enzymatic activity. Clearly, the carbon nanofibers prepared using covalent functionalization yield the overall highest activity, giving an enhancement in activity of a factor of 10 in the initial rate (Figure 3b) and by a factor of 3 after 40 min (Figure 3c).

Electrochemical Characterization of Cyt *c*-Modified Electrodes. After establishing that active cyt *c* was effectively immobilized on undecylenic acid functionalized nanofiber electrodes, we investigated how the electrochemical response of cyt *c* on these higher surface area electrodes compared with the response of similarly modified gold and glassy carbon. Samples of VACNFs, glassy carbon, and gold were functionalized with undecylenic acid and MUA,

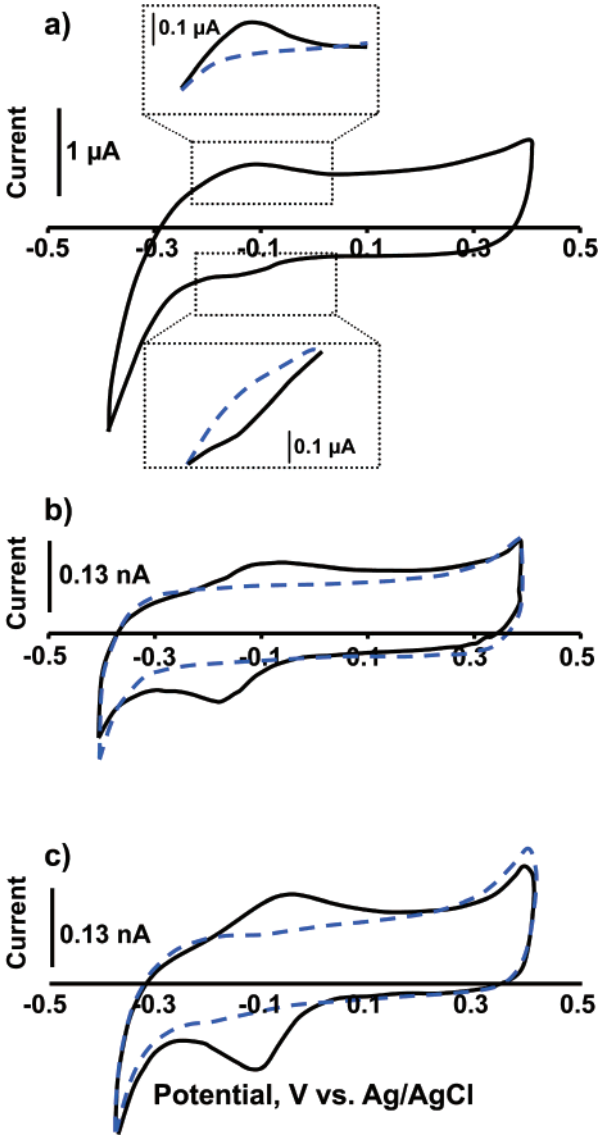

Figure 4. Cyclic voltammetry of cyt *c* on carboxylic acid-terminated surfaces of (a) VACNF, (b) glassy carbon, and (c) gold electrodes. The solid lines are voltammograms with cyt *c* immobilized onto the electrodes; the dashed lines are background voltammograms taken before cyt *c* was introduced into the cell.

respectively, and cyclic voltammograms were measured before and after immobilizing cyt *c* on the surfaces. In the flow cell design, this can be accomplished without moving the sample, facilitating direct comparison. Figure 4 shows representative cyclic voltammograms of the resulting cyt *c*-modified surfaces, measured in 4.4 mM PB, pH 7.0. Data reported here were obtained at a sweep rate of 50 mV/s and are presented as the total current flowing in the ~2 mm diameter region of sample exposed to the electrolyte. Additional data (not shown) were also obtained at other sweep rates, but we found that the oxidation and reduction peaks on the VACNF samples were most easily observable at this sweep rate.

Figure 4a shows cyclic voltammograms of the VACNFs that were modified with carboxylic acid groups after immobilization with cyt *c* (solid line). Because the differences between these spectra are small, Figure 4a shows expanded graphs of the oxidation and reduction peaks for the sample before cyt *c* was added (dashed line) and after it was added

(32) Malmgren, L.; Olsson, Y.; Olsson, T.; Kristensson, K. *Brain Res.* **1978**, *153*, 477.

(solid line). While the background scan (dashed) is essentially featureless, after immobilization of cyt *c* the oxidation sweep shows a clear oxidation peak with an maximum amplitude of ~100 nA, reached at a potential of −0.099 V, and the reduction sweep shows a downward peak with maximum amplitude at −0.128 V. The average of the potentials at which peak anodic and cathodic currents are observed should be equal to the formal potential, E_0'. These data yield an $E_0' = -0.114$ V and a separation ΔE between oxidation and reduction peak maxima of ~30 mV. Repeated measurements of multiple samples show some variability in the peak separation due to the small size of the peaks and the sloping background; however, the measurements all yield ΔE in the range of 30−50 mV. This small peak separation indicates efficient electron transfer at the nanofiber−electrolyte interface even on functionalized samples.

For comparison, Figure 4b shows cyclic voltammograms measured on surfaces of glassy carbon that were functionalized with carboxylic acid groups in a manner identical to thatof the VACNFs. After immobilization of cyt *c* (solid line) the voltammogram shows oxidation and reduction peaks at −0.067 and −0.181 V, respectively, while the corresponding background scan measured before cyt *c* immobilization (dashed line) is featureless. The peaks yield a formal potential $E_0' = -0.124$ V and a separation $\Delta E = 113$ mV. Finally, Figure 4c also shows data for a gold surface functionalized with MUA. In this case the oxidation and reduction peaks are at −59 mV and −130 mV, yielding $E_0' = -0.094$ V and $\Delta E = 71$ mV.

The presence of the oxidation and reduction waves demonstrates the presence of electrochemically active cyt *c* on the surfaces. The observed redox potentials are shifted from those of free cyt *c* in solution but are similar to those reported previously for cyt *c* on carboxylic acid-terminated surfaces of gold, glassy carbon, and carbon nanotubes[12,14,20,33−37] after taking into account possible differences in the reference electrodes.

At negative potentials the cyclic voltammogram of the carbon nanofiber sample shows more background current. While the origin of this remains under investiation, one possibility is a lower overpotential for H^+ reduction on nanofibers compared with planar samples. This increased background makes the reduction peak of cyt *c* more difficult to discern than the oxidization peak. A second important feature of the nanofiber surfaces is that the peak separation of ~30−50 mV is significantly smaller than the values that we obtained on glassy carbon and gold. This suggests that the nanofiber surfaces provide unusually good electrochemical reversibility.

We performed further control experiments to ensure that the peaks shown in Figure 4a arise from direct electron transfer between the adsorbed protein and the carboxylic acid functionalized VACNFs and not to any other sources such as cyt *c* adsorption elsewhere in the electrochemical cell. Because the ABTS assay showed that amine- and alkane-terminated surfaces adsorb only negligible quantities of active protein, we also examined the electrochemistry of cyt *c* introduced to the amine- and alkane-modified VACNF surfaces as the working electrodes. The cyclic voltammograms of these samples before and after exposure to cyt *c* were identical, showing no discernible electron transfer with the protein. Thus, the chemical and electrochemical data agree, both showing that there is negligible active cyt *c* on alkane- and amine-terminated nanofiber surfaces. Functionalization of the VACNF surfaces with well-defined carboxylic acid groups greatly facilitates the detection.

Table 2. Capacitive Currents on Functionalized and Unmodified VACNF, Glassy Carbon, and Gold Electrodes and Anodic Peak Currents Due to Adsorbed Cyt *c* on Carboxylic Acid-Terminated Electrodes[a]

material	capacitive current (nA)	peak current (nA)
COOH−VACNF	1500 ± 430	91 ± 24
bare VACNF	1400 ± 430	
COOH−glassy carbon	14 ± 4	4 ± 0.01
bare glassy carbon	85 ± 9	
COOH−gold	15 ± 4	8 ± 0.8
bare gold	232	

[a] Standard deviations reflect estimated uncertainties based on replicate measurements of two to three samples.

We were able to directly detect adsorbed cyt *c* (reversible redox waves) on the carboxylic acid-terminated VACNF, glassy carbon, and gold surfaces. One major difference in the electrochemical properties of these different surfaces was the cathodic and anodic peak heights. These were calculated by finding the peak current value and subtracting the background current value at the same potential. The average anodic peak height values are shown in Table 2 and graphically depicted in Figure 5. The left-hand side of the graph shows the magnitude of the peak current due to cyt *c* on VACNFs. The peak current due to redox of cyt *c* was approximately 10 times higher on undecylenic acid-modified VACNF surfaces than on undecylenic acid-modified glassy carbon or gold. This higher peak current is a direct result of the fact that the higher surface area of the nanofibers enables electrochemical sampling of 10 times more immobilized cyt *c*. In fact, the electrochemical signal enhancement on VACNFs we observe here for cyt *c* is is nearly identical to the enhancement in the biologically accessible area we measured previously using the biotin−avidin system.[5]

One characteristic of the VACNF cyclic voltammogram of cyt *c* that is immediately evident from Figure 4a is that

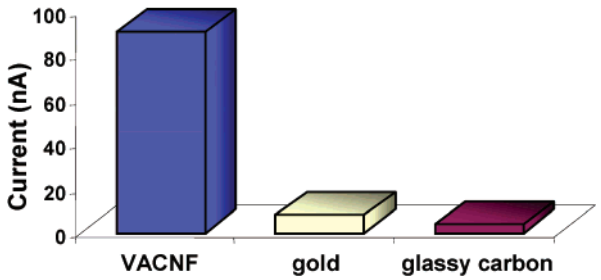

Figure 5. Peak anodic currents due to cyt *c* adsorption on carboxylic acid-terminated surfaces of VACNFs, glassy carbon, and gold.

(33) Petrovic, J.; Clark, R. A.; Yue, H.; Waldeck, D. H.; Bowden, E. F. *Langmuir* **2005**, *21*, 6308.
(34) Rikhie, J.; Sampath, S. *Electroanalysis* **2005**, *17*, 762.
(35) Yin, Z.-Z.; Zhao, G.-C.; Wei, X.-W. *Chem. Lett.* **2005**, *34*, 992.
(36) Zhao, G.-C.; Yin, Z.-Z.; Zhang, L.; Wei, X.-W. *Electrochem. Commun.* **2005**, *7*, 256.
(37) Wang, J.; Li, M.; Shi, Z.; Li, N.; Gu, Z. *Anal. Chem.* **2002**, *74*, 1993.

while the absolute size of the redox current is greater than those of the other surfaces, it is more difficult to discern the redox peaks associated with the bound protein above the capacitive current.

To help understand why the redox peaks are less apparent on the nanofiber surfaces, we compared the capacitance (which gives rise to the background current) of unmodified glassy carbon, gold, and VACNF surfaces to their undecylenic acid-modified analogues using cyclic voltammetry. The unmodified, or "bare" glassy carbon and gold surfaces were generated by immersion in a piranha bath[22] and then rinsing with deionized water before the electrochemistry. Bare VACNF surfaces were used as grown. Table 2 shows the resulting capacitance currents. These data show that surfaces of gold and glassy carbon that were functionalized with undecylenic acid exhibited 6−10 times lower capacitive current than unmodified surfaces. In contrast, functionalization of VACNFs has almost no effect on the capacitance. The fact that functionalizing the VACNFs with an alkyl layer does not significantly reduce the capacitive current indicates a lower surface coverage or packing density of the alkyl chains on the VACNFs compared to the monolayers formed by the same chemistry on glassy carbon. The net result is that in going from planar glassy carbon to nanofibers, there is a 100-fold increase in capacitance; this can be roughly ascribed to a 10-fold increase due to the increased surface area of the nanofibers and another 10-fold increase due to the increased porosity of the molecular functionalization layers on nanofibers compared with glassy carbon.

Discussion

Detection of electrochemical currents associated with adsorbed proteins is a complex process, as the measured signals depend on a number of chemical, biological, and electrical factors. Ideally, one would expect that the high surface area of carbon nanofibers could be used to enhance electrochemical detection simply through an increased surface area effect.[38,39] Our data show that the situation is more complex. Colorimetric analysis clearly shows that the undecylenic acid-modified nanofiber samples adsorb significantly more enzymatically active cyt *c*. For example, the nanofibers modified with cyt *c* were found to oxidize ABTS at 10 times greater initial rates than glassy carbon modified with cyt *c*. The absolute redox current observed on the nanofiber samples is also higher than the currents observed on surfaces of glassy carbon or gold. However, the capacitive background signal of the VACNF samples is also very high. The ability to detect electron transfer with the heme group in the protein on VACNFs is controlled largely by this capacitive background. To the achieve highest signal-to-noise ratio, one desires an electrode surface that has low capacitance while still permitting facile electron transfer from the electrode to the protein.

Previous studies have identified a number of factors that control the electrochemical response of enzyme- and protein-modified surfaces. Electrochemical detection of cyt *c* with carbon-based electrodes containing a high proportion of basal planes such as graphite[34] and carbon nanotubes[35,37] has required first "activating" the surfaces by intentional oxidation and/or by electrochemical cycling. This procedure leads to surface oxidized sites, including carboxylic acid groups, that enhance the binding of cyt *c* through electrostatic interactions; however, it can also modify the microscopic structure of the surface, often by inducing oxidation at basal plane sites to expose edge planes. With these oxidation processes it is difficult to distinguish whether changes in electrochemical response arise from changes in structure (such as oxidation of basal plane sites to expose edge planes) or changes in surface chemistry. The use of covalently linked molecular layers provides a way to more controllably tune the number, type, and electrochemical properties of chemical functional groups at the surface. For example, covalently attached molecular layers enable control over the electrochemical characteristics such as the capacitance[40] and selectivity of the molecular layer,[41,42] as well as the ability to generate mixed monolayers for greatest control over protein binding and orientation.[11]

Previous studies of bare graphitic electrodes have shown that electrodes that expose the edge planes of graphite have much higher electron-transfer rates and higher capacitance than the electrodes consisting of basal planes.[43] In fact, edge planes and defect sites have been suggested to be the primary electron-transfer regions in carbon materials, responsible for all observed electrode activity.[44] Carbon electrodes modified with cyt *c* also show signal enhancement at edge planes.[45] However, the differences between edge and basal planes arise also because the coordinatively saturated basal plane does not easily oxidize, while the more facile oxidation of the edge planes provides greater coordination to cyt *c* and a higher density of redox-active sites.[10,45] Consequently, the differences in electrochemical properties between edge and basal planes are a convolution of the chemical and electrochemical properties of these surfaces.

With carbon nanofibers, previous studies and our own TEM studies show that the walls of the nanofibers contain large numbers of cut edge planes; estimates from TEM measurements yield one cut edge plane every 1−3 nm along the length of the nanofiber. Thus, nanofibers expose both basal planes and edge planes.

In a previous study we showed that the electrically active surface area of *unmodified* (bare) VACNFs was approximately 10 times higher than that of an unmodified flat glassy carbon electrode of the same geometric area.[5] A similar increase in accessible surface area was observed in chemical measurements in which we quantitatively measured the amount of avidin that would bind to nanofibers functionalized

(38) Roy, S.; Vedala, H.; Choi, W. *Nanotechnology* **2006**, *17*, S14.
(39) Guiseppe-Elie, A.; Lei, C.; Baughman, R. H. *Nanotechnology* **2002**, *13*, 559.
(40) Finklea, H. O.; Avery, S.; Lynch, M. *Langmuir* **1987**, *3*, 409.
(41) Clare, T. L.; Clare, B. H.; Nichols, B. M.; Abbott, N. L.; Hamers, R. J. *Langmuir* **2005**, *21*, 6344.
(42) Malem, F.; Mandler, D. *Anal. Chem.* **1993**, *65*, 37.
(43) McDermott, M. T.; McDermott, C. A.; McCreery, R. L. *Anal. Chem.* **1993**, *65*, 937.
(44) Banks, C. E.; Davies, T. J.; Wildgoose, G. G.; Compton, R. G. *Chem. Commun.* **2005**, 829.
(45) Armstrong, F. A.; Bond, A. M.; Hill, H. A. O.; Psalti, I. S. M.; Zoski, C. G. *J. Phys. Chem.* **1989**, *93*, 6485.

with the complementary molecule biotin. Our present measurements show that nanofiber electrodes functionalized with cyt *c* also give approximately 10 times higher redox current than flat electrodes. The capacitance of the bare (unfunctionalized) electrodes also appears to scale by this same factor. Yet, the capacitance of the functionalized nanofibers is unexpectedly high.

We believe this unexpectly high capacitive background observed for the functionalized carbon nanofibers arises primarily from a decreased density of the molecular functionalization layers. Our data (Table 2) show that functionalization of carbon nanofibers using undecylenic acid has very little effect on the interfacial capacitance, while functionalization of glassy carbon with the same molecule leads to a pronounced decrease in capacitance. Becuase nanofibers and glassy carbon both comprise graphitic domains, these differences are surprising. X-ray photoelectron spectroscopy data and previous work on functionalized nanofibers both suggest a high degree of functionalization. Yet, the microscopic structure of the carbon nanofibers and glassy carbon are very different. First, the sizes of the graphitic domains on the type II glassy carbon used here are most likely larger, estimated to be 5−7 nm.[46] In contrast, TEM measurements of our nanofibers show both basal planes and cut edge planes exposed at the nanofiber sidewalls, with exposed edge planes approximately every 1.5−2.5 nm. Because the van der Waals diameter of an alkyl chain is only 4.6 Å, preferential binding of molecules at the edge sites on nanofibers would lead to a very open molecular film.

Raman measurements have been used previously to characterize the amount of basal and edge planes in bulk glassy carbon[47] and carbon nanotubes[48] via the ratio of intensities of Raman features at 1360 cm^{-1} (commonly referred to as the "D band") and that at 1582 cm^{-1} (the E_{2g}, or "G" band). We have obtained Raman spectra of nanofibers and glassy carbon samples, which are presented in Supporting Information. The Raman spectra reveal distinctly different peak shapes for these two materials. However, at the present time a quantitative comparison cannot be made because while glassy carbon is essentially uniform on optical length scales, the cylindrical shape of the vertically aligned nanofibers leads to very different electromagnetic coupling parallel and perpendicular to the axis of each nanofiber. Consequently the effective excitation probabilities of two modes are not presently known.

An important conclusion that can be drawn is that the molecular functionalization layer plays two roles. One is to provide binding sites (carboxylic acid groups) for cyt *c* immobilization and orientation. A second is to reduce the capacitive background. Self-assembled monolayers on gold have been claimed to simultaneously reduce charging currents while permitting faradic electron transfer to the electrode surface, resulting in an increased signal-to-noise ratio.[49] To optimize the utility of carbon nanofibers for enzymatic sensing, it will be necessary to optimize the monolayer properties to achieve increased density to reduce capacitive background. Another feasible option is to use the VACNFs to fabricate nanoelectrode arrays, which exhibit lower charging currents.[50] The studies presented here show that functionalization of the nanofibers with well-defined molecular monolayers provides a way to control the interactions of the proteins with the surfaces and that nanofibers functionalized with monolayers having terminal carboxylic acid groups can be used to immobilize active metalloproteins.

Conclusion

Our results show that photochemical functionalization of carbon nanofibers with carboxylic acid groups leads to successful imobilization of the metalloprotein cyt *c*. Chemical measurements using ABTS and electrochemical measurements of the redox activity both show show ∼10 times enhancements in activity compared with planar surfaces. This ∼10 times enhancement closely parallels previous measurements of the microscopic surface area enhancement, indicating that the observed activity increase on nanofibers reflects the increased microscopic surface area, most of which is associated with the nanofiber sidewalls. While the high surface area of the nanofibers allows the adsorbed cyt *c* molecules to produce a large increase in electrochemical current, high capacitive currents due to the high surface area and a leaky monolayer on the VACNFs partially obscured this higher signal and partially offset the potential improvement in the signal-to-noise ratio. These findings demonstate the ability to use VACNFs as high surface area electrodes for biological detection with metalloproteins, while also underscoring the importance of the surface functionalization layers in controlling the overall electrochemical response.

Acknowledgment. This work was supported in part by the National Science Foundation Grants DMR0210806 and CHE0314618.

Supporting Information Available: Raman spectra of carbon nanofibers and of glassy carbon (PDF). This material is available free of charge via the Internet at http://pubs.acs.org.

CM0609000

(46) McCreery, R. L. Carbon Electrodes: Structural Effects on Electron Transfer Kinetics. In *Electroanalytical Chemistry*; Bard, A. J., Ed.; Marcel Dekker: New York, 1991; Vol. 17, p 221.
(47) Wang, Y.; Alsmeyer, D. C.; McCreery, R. L. *Chem. Mater.* **1990**, *2*, 557.
(48) Dresselhaus, M. S.; Dresselhaus, G.; Saito, M.; Jorio, A. *Phys. Rep.* **2005**, *409*, 47.
(49) Finklea, H. O. Electrochemistry of Organized Monolayers of Thiols and Related Molecules on Electrodes. In *Electroanalytical Chemistry*; Bard, A. J., Rubinstein, I., Eds.; Marcel Dekker: New York, 1996; Vol. 19, p 110.
(50) Arrigan, D. W. M. *Analyst* **2004**, *129*, 1167.